Available online at BCREC website: https://bcrec.id

Bulletin of Chemical Reaction Engineering & Catalysis, 15 (3) 2020, 765-785

Research Article

Study of the Interaction of Heavy Metals (Cu(II), Zn(II)) Ions with a Clay Soil of the Region of Naima-Tiaret-Algeria

Taibi Mohamed[1], Elaziouti Abdelkader[1,*], Laouedj Nadjia[2], Dellal Abdelkader[3]

[1]Laboratoire des Sciences Technologie et Génie des Procédés (L.S.T.G.P.), Faculté de Chimie, Université des Sciences et de la Technologie d'Oran Mohammed Boudiaf (USTO M.B.) BP 1505 El M'naouar 31000 Oran, Algérie.
[2]Laboratoire de Chimie des Matériaux Inorganiques et Application (L.C.M.I.A.), Université des Sciences et de la Technologie d'Oran Mohammed Boudiaf (USTO M.B.). BP 1505 El M'naouar 31000 Oran, Algérie.
[3]Directeur de Laboratoire d'Agro-biotechnologie et de Nutrition en Zones Semi-arides, Université Ibn Khaldoun Tiaret, Algérie Tiaret, Algérie.

Received: 26th August 2020; Revised: 9th October 2020; Accepted: 9th October 2020; Available online: 10th October 2020; Published regularly: December 2020

Abstract

The RM (RM stands for the pristine clay) collected from sites in the Naima-Tiaret-Algeria and its purified phase TM (TM stands for the treated clay) were characterized using XRF, XRD, FT−IR, SEM−EDX, and DC electrical conductivity techniques. The as-prepared clays were used as potential adsorbents for the removal of Cu^{2+} and Zn^{2+} metals ions. Highly purified clay TM, exhibiting a basal, spacing of 25.83 Å and CEC of 51 meq/100 g, was obtained. The type of interstratified I/M in the studied sites is S=1, based on the calculation method of Watanabe. The percentage of illite type S=1 is between 80−85% illite. The adsorption equilibrium was established in 60 min with the capacities of 28.57 and 24.39 mg/g for Cu^{2+} onto RM, 32.25 and 4.95 mg/g for Zn^{2+} in the presence of TM. D-R isotherm model was more suitable with the adsorption process than Freundlich and Langmuir models suggesting the ion exchange nature of the retention mechanism in most cases (E > 8 kJ/mol). Pseudo second-order model best described the kinetics of adsorption process. The adsorption mechanism was mainly monitored by ion exchange mechanism between exchangeable interlayer cations (Na) in the interstratified I/M and Cu^{2+} or Zn^{2+} metals from aqueous matrix. Further, the release of H^+ ions from the edge of the layer structure in acidic environments promote the adsorption of heavy metals onto the surfaces interstratified I/M clay soils via electrostatic attraction.

Keywords: Interstratification Illite/Montmorillonite; Clay Soil; Heavy metals; Adsorption; Kinetics; Cu(II); Zn(II)

How to Cite: Mohamed, T., Abdelkader, E., Nadjia, L., Abdelkader, D. (2020). Study of the Interaction of Heavy Metals (Cu(II), Zn(II)) Ions with a Clay Soil of the Region of Naima-Tiaret-Algeria. *Bulletin of Chemical Reaction Engineering & Catalysis*, 15(3), 765-785 (doi:10.9767/bcrec.15.3.8773.765-785)

Permalink/DOI: https://doi.org/10.9767/bcrec.15.3.8773.765-785

1. Introduction

The term "heavy metal" is often used for the group of elements that are associated with environment pollution and have potential toxic effects on wildlife. According to the latest recommendations of the competent international bodies, classification of metals on heavy and light should be based not only on the periodic table of elements and their chemical properties, but also on assessment of the impact of toxic metals in the environment [1]. Heavy metals are the ma-

* Corresponding Author.
E-mail: elaziouti_a@yahoo.com (E. Abdelkader);
Tel: +213-05-40288630, Fax: +213-41-500056

jor components of inorganic pollutants comes from the industrial activity, such as: pesticides, fertilizers, sludge, electroplating, battery manufacture, metal extraction and municipal solid wastes, which are considered a primary source of pollution of the water, land, plants and animals [2]. Many heavy metals (copper, zinc, manganese and iron) are essential for all living organisms, since they play an important role as active centers of an enzyme and as essentiel substances in mammalian metabolic systems, for instance, zinc plays a cruciale role in the development of the brain and intelligence; copper is a constituent element of hemocyanin in human body; manganese can promoting the normal growth and development of bone, and maintain the normal metabolism of glucose and fat. However, in higher concentrations than optimal, they are harmful. Thus, the heavy metals are classified into three groups, for example, potentially toxic groupings (mercury, cadmium, arsenic and lead), normal harmful groupings (nickel, zinc, copper, chromium), and less poisonous groupings (molybdenum, manganese and iron) [3]. The regular and arbitral releases of these harmful heavy metals in wastewater causes serious environmental, social and economic impacts. Thus, heavy metal pollutants have been à topic of intensive research to their connection with health hazards for all organisms due to its toxicity, persistence, recalcitrance, non-biodegradable, bioaccumulation and biological amplification in the food chain [4].

Most heavy metals even at low concentration or high trace element unbalances exhibit harmful effects on the organisms due to their high carcinogenic and mutagenic impacts on wildlife [5]. Thus, the withdrawal of heavy metals form industrial and urban wastewater is a big environmental concern to provide a metal free water resource. Conventional processes for removing dissolved heavy metals, including ion exchange, chemical precipitation, membrane filtration technologies, electrochemical treatment, phyto-extraction, ultrafiltration, reverse osmosis and electro-dialysis technologies. However, most of these processes face various challenges and limitations, such as: a high cost, high-energy consuming, complicated equipments, ineffective at low metal concentrations and long reaction time [6]. From all these processes, the adsorption process is one of the best, efficient, low-cost, green environmentally friendly, and ease of operation technique for removing dissolved metal ions from wastewaters [7]. Right now, various materials have been proposed to remove heavy metal form wastewater including activated carbon, bentonite, kaolin, clays, zeolite, algae, diatomite, layered double hydroxides (HDLs), advanced oxidation processes (AOPs) and the emerging metal-organic frameworks (MOFs) [2,6,8]. Activated carbon is effective material in the removal of heavy metals from wastewater due to its high metal ions adsorption capacity. However, these adsorbent materials have disadvantages, such as: harmful byproducts and high treatment cost [8]. Some researchers have focused on using clay soils due to its unique characteristic, such as: availability, low cost, versatile metal composition, chemical and mechanical stability, colloidal properties, chemically active surface, re-active interfoliar space, Brønsted and Lewis acidity, high cation exchange capacity (CEC) and great surface area [9].

Clay minerals are mostly phyllosilicate minerals, which are described by layered structural units composed of polymeric sheets of SiO_4 tetrahedra linked to sheets of (A1, Mg, Fe)$(O,OH)_6$ octahedra. They are found in the clay-size fraction of sediments and soils <2 μm. The tetrahedral sheets have a $Si_2O_6(OH)_4$ unit consisting of four hydroxyl groups surrounding every silicon atoms in a tetrahedron coordination. By contrast, an octahedral coordination consists of Fe, Mg or Al atoms surrounded by six hydroxyl or oxygen atoms, such as in the composition of $Al_2(OH)_6$. The silicate clay minerals composition changes regularly due to substitution of ions within the mineral structure. The process of replacing one structural cation for another of similar size is referred to as isomorphous substitution. This replacement represents the primary source of both negative and positive charges in clay minerals. For instance, the substitution of one Al^{3+} for a Si^{4+} in the tetrahedron results in a gain of one negative charge and widely impolies in the removal of heavy metal cations from wastewater. Alternatively, replacement of a lower valence cation by one with a higher valence (Fe^{2+} by Fe^{3+}) gives rise to a gain of one positive charge. In most soils, however, substitutions that result in net negative charge exceed those producing a positive charge [9].

Heavy metal removal by clay soils and clay composites consists of a series of complicated removal mechanisms, such as: ion exchange, surface complexation, and direct bonding of heavy metal cations to the surface of clays [10]. Removing of heavy metal by bentonite with respect to Cu^{2+}, Zn^{2+} and Pb^{2+} were studied by Karimi and Salem [11]. They concluded that the release of H^+ ions from the edge of the of

the layer structure in acidic environments boosts the adsorption of heavy metal ions from wastewaters. Bhattacharyya and Gupta [12] indicated that kaolinite is able to remove various heavy metals like Hg^{2+}, Cd^{2+}, Cu^{2+}, and Pb^{2+} effectively in aqueous solution due to its H^+ ions released from the edge of the structure in acidic conditions and surface adsorption on the exposed tetrahedral or octahedral sheets. Wang *et al.* [13] investigated the removal capacity of heavy metals ions in aqueous solution, using acid-activated montmorillonite. The modification by acid activation assistances alter the surface area, increases the sorption sites, enhances thermal stability and adsorption capacity. The sorption process for cadmium and copper from aqueous solutions using activated coal was assessed by Rao *et al.* [14] and 20 mg/g of Cd^{2+} and Cu^{2+} were highly up taken. The up take capacity of heavy metals ions like Cr^{3+}, Cd^{2+}, Cu^{2+} and Pb^{2+} using Jordanian zeolite was investigated studied by Baker *et al.* [15]. The Jordanian phillipsite tuff exhibited high selectivity for the discharge of Pb^{2+} about 98% achieved within 90 min, then Cr^{3+}, Cu^{2+} and Cd^{2+} about 96% achieved within 5 h. Mishra and Patel [16] studied the use of activated carbon, kaolin, bentonite, blast furnace slag, and fly ash as adsorbent to remove the lead and zinc ions from water. From their results, it was found that bentonite and fly ash were effective for lead and zinc removal. Aytas *et al.* [17] investigated the effect of various key parameters (pH, contact time, temperature, and initial metal concentration on uranium (U(VI)) adsorption) on thermally activated bentonite (TAB). It was found that when bentonite was calcinated at 400 °C, the adsorptive capacity is highest but decreases when above 400 °C. The TAB has a maximum sorption at pH 9.0. It was shown that the percentage sorption of uranium at the optimum adsorption conditions was found as 66.2±0.7%. Oliveira *et al.* [18] prepared clay iron oxide composite for adsorption of metal ions Ni^{2+}, Cu^{2+}, Cd^{2+}, and Zn^{2+} from aqueous solution. They compared the metal adsorption capacity of bentonite clay and its magnetic composite. They showed that the presence of iron oxide increased the adsorption capacity of the bentonite. These adsorbents showed the advantage to be easily removed from the medium by a simple magnetic separation procedure after saturation is reached.

As deduced from the above literature review, clay materials have been applied to uptake various heavy metals ions from simulated wastewater due to its availability, large surface area and expandable layered structure, and the high adsorption capacity. Algeria possesses enormous reserves of clay soils in the region of Naima-Tiaret. The soil of NAIMA is basic completely devoid of limestone, more or less rich element (potassium, sodium), and organic matter. These sites are operated by local people, mainly for the manufacture of various potteries. Based on the above highlights, the clay soils located in the region of Naima-Tiaret, Algeria, as shown in the Figure 1, are used as potential adsorbents for the removal of two heavy metal ions such as Copper (Cu^{2+}) and zinc (Zn^{2+}) in the simulated aqueous solution. We examined the adsorption of these heavy metals which could pollute the waters, the adsorbates used are metallic trace elements, the choice of these two metals has been motivated, first, by the dangers to their health and the environment and, secondly, the ease of their determination in water. Zinc (Zn) is the most toxic. Indeed, it is now recognized that the toxicity increases gradually as the amount released increases. Copper (Cu) production has increased in recent decades and thus the amounts of copper in the environment increased.

To the best of our information, there is no work have been stated on the use of the Naima clay soils as an adsorbent for these heavy metal ions. The pristine and chemically treated clays were characterized by different tech-

Figure 1. Map showing the locations of the clay deposits (Algeria, Tiaret-Naima).

niques including X-ray fluorescence (XRF), X-ray diffraction (XRD), Fourier transform infrared (FT−IR), scanning electron microscope with energy-dispersive X-ray (SEM−EDX) and DC electrical conductivity techniques. The variation $\Delta 2\theta_1 - \Delta 2\theta_2$ method of Watanabe was used to determine the type and percentage interstratification illite/montmorillonite. The impact of two key parameters (contact time and initial metal ion solution concentration) on the removal process of these heavy metals onto clay materials was investigated in detail. Three adsorption isotherm models, such as Langmuir, Freundlich and Dubinin–Radushkevich (D–R) isotherm were applied to the equilibrium data to explain the main interactive mechanisms implicated in the sorption process. For better description of the adsorption mechanism, kinetic data were correlated with the pseudo-first-order and pseudo-second-order models. The mechanism of the enhanced adsorption efficiency of our materials towards Cu^{2+} or Zn^{2+} metal ions from aqueous matrix was investigated in details. Finally, a comparison study between the adsorption capacity of our clays towards Cu^{2+} and Zn^{2+} metals and those removed by various clay materials from previous relevant studies was highlighted.

2. Materials and Methods

Clay soil was obtained from clay deposits located in the region of Naima-Tiaret, Algeria. The clay sample was disintegrated mechanically and passed through the sieve of 2 mm. The sifted sample in the tray (small sizes) is used for the batch study (is denoted as untreated clay; RM). The preliminary treatments of the natural clay soils were performed by washing with distilled water to remove impurities and organic species, drying in oven at 105 °C for 24 h to eliminate moistures and then sodium hominization to replace all the exchangeable cations by sodium cations (Na^+) to obtain good clay colloidal dispersions and expandable layered structure with the well-defined size fractions, smaller than 2 micron. The <2 μm particle size fraction was filtered, and then washed several times with distilled water until free Cl^- was not detected in the suspension ($AgNO_3$ test). The <2 μm fraction was collected by centrifugation, dried at 60 °C for 24 h and grinded (is denoted as chemically treated clay; TM) to be used for the batch investigation.

2.1 Determination of the Cation Exchange Capacity (CEC)

In a series of Erlenmeyer flasks, we introduce a constant volume of a clay suspension concentration equal to 1 g/L and varying amounts of methylene blue, the various mixtures are stirred normal hang one hour at room temperature. Balance after the suspensions were centrifuged and the solutions of methylene blue were measured by residual UV-Visible spectrophotometry at a wavelength of 665 nm. The isotherm is obtained by plotting the amount of methylene blue set according to the residual concentration.

2.2 Acid-base Surface Properties

Solid surface properties were determined by potentiometric titration. The titration was carried out using 0.01 M potassium hydroxide (KOH) in a 0.01 M NaCl electrolyte solution. The solid surface electrostatic charge results from an acid-base surface reaction. These are correlated by the mass conservation equation, based on the reactions of surface hydroxyl groups. For each acid-base titration point, the surface charge Q is obtained from following expression equation (1):

$$Q = \frac{\left(-C_b + \left[OH^-\right] - \left[H^+\right]\right)}{m} \quad (1)$$

where Q (mol/g) is the surface charge, C_b (mol/L) is the amount of base added and m (g/L) is the test sample. We can therefore obtain the average surface charge of the solid Q as a function of the pH. The results obtained for test portion (m = 0.1 g/L).

2.3 DC Conductivity

The DC conductivity of clay samples were measured using a bridge (LCR-821, Instek LCR meter) with the frequency (f) between 104 and 106 Hz. The samples after preparationin the hydraulic hot press (300 bars) as the disk with dimension 1–2 mm thick and 12 mm in diameter were inserted between the two platinum parallel plate electrodes isolated from each other using the Teflon film sandwiched the sample. The instrument measures resistance via two-probe technique and the resistivity and conductivity are calculated according to this equation equation (2):

$$\sigma = \frac{e}{VS} I \quad (2)$$

where I, V, S and e are current, applied voltage (50 Hz), sample area and sample thickness, respectively. The instrument is connected with the heated chamber and temperature controller to increase the temperature of the samples from 300 and 440 K with a step of 2 K/min. All

system is attached to the standard PC monitor, Windows Private Software accessible via the RS-232 terminal.

2.4 Preparation of the Cu and Zn Solution

For all the metals studied, we used the same method of preparation of a stock solution, from which we prepare a series of well-defined solution concentrations via successive dilution. Two stock solutions are prepared from the salt precursors: ($ZnCl_2$, 0.5 g/L, Zn) for zinc and ($CuSO_4$, 0.5 g/L, Cu) for copper, then a volume of stock solution is required each time and we vary the initial concentrations of metal ions by solution by successive dilution with distilled water. For each concentration of the metal ion mixing 50 mL of the diluted solution with the (RM or TM) clay mass at 100 mg thereafter, the contents of the flask were centrifuged at 4000 rpm for 30 min and then determined by atomic absorption.

2.5 Batch Adsorption

Batch adsorption is a simple technique commonly used to assess the adsorption capacities of natural and synthetic sorbents. In addition to its easy handling, it makes it possible to bring out important information on the effectiveness of a given sorbent in eliminating the solute studied in static conditions. Batch adsorption is therefore widely used for environmental purposes, notably for the treatment of waste water. The adsorption of the selected metal ions was carried out at various initial concentrations of 10 to 100 mg/L, pH 5.7 and stirring speed of 300 rpm in equilibrium time of 60 min. 2 g/L of each RM (pristine) and TM (treated) samples were placed in an Erlenmeyer flask containing metal ions of known concentration. The pH of the metal solution was adjusted before mixing with the adsorbent with 0.1 M HCl and 0.1 M NaOH. The samples were shaken at 200 rpm for 60 min to reach adsorbent-adsorbate equilibrium. The suspension was then centrifuged and 10 mL of supernatant was filtered. Finally, the resulting solution samples were stored at 4 °C until the Cu(II) and Zn(II) metal concentration was measured using Spectr. AA 50/55 S Atomic Absorption spectrophotometer. The amount of heavy metal removed was calculated from the difference between the initial and final concentration using the following equation (3) and percentage removal was obtained using equation (4):

$$Q_e = \left(C_0 - C_e\right)\frac{V}{m} \tag{3}$$

$$\%removal = \frac{\left(C_0 - C_e\right)}{C_0} \times 100 \tag{4}$$

where Q_e is the equilibrium adsorption capacity (mg/g), C_0 and C_e are the initial and equilibrium metal concentrations (mg/L) respectively, V is the volume of solution (L) and m is the mass of the adsorbent (g).

2.6 Characterizations

X-ray diffraction (XRD) analysis was carried out using a siemens D 5000 automatic diffractometer with Cu-Kα radiation (λ = 0.154178 nm) and including a rear monochromator to eliminate the fluorescence of iron. The front and rear windows were fixed at 2 mm, plus an additional 0.2 mm rear slit. A low speed of rotation (0.01° s^{-1}) was selected to obtain well defined spokes over 10−80° for the both RM and TM samples. FT−IR spectrum was performed using a spectrometer Shimatzu 8400 over a range of 400 to 4500 cm^{-1} with a resolution of 2 cm^{-1}. The samples were packaged in the form of dispersion in a KBr pellet (1/200) by weight. The powder morphology and elemental composition were obtained using a FEI Quanta 650 Scanning electron microscope (Bruker Nano GmbH Berlin. Germany) linked with a BRUKER XFlash 6/10 editor for energy-dispersive X-ray (SEM−EDX) analysis. Elemental analysis of crude and purified clays was obtained using a Bruker S1 Titan X-ray fluorescence (XRF) spectrometer. The conductivity measurement was done by using Instek 821 LCR meter with controlled temperature between 300 and 440 K with a step of 2 K/min. The optical density analysis was performed on a spectrophotometer agile model driven by a 8543 computer. The peak wavelengths are obtained directly by automatic scanning between 200 and 800 nm.

2.7 Kinetic Modelling

The experimental kinetic data are investigated by the pseudo-first-order model according to the Lagergren's equation [19] equation (5):

$$\ln\left(Q_e - Q_{et}\right) = \ln Q_e - k_1 t \tag{5}$$

where k_1 is the rate constant of pseudo-first-order kinetics (min^{-1}) and Q_{et} is adsorption capacity at time t (mg /g). Hence, the values of k_1 and Qe are deduced from the slope (k_1) and the intercept ln (Q_e) of the linear plots of ln (Q_e−Q_{et}) versus t.

The kinetic data were further analyzed using pseudo-second-order model, as follows [20] equation (6):

$$\frac{t}{Q_{et}} = \frac{1}{k_2 Q_e^2} + \frac{1}{Q_e} t \quad (6)$$

where k_2 is the rate constant of the pseudo-second-order ($g.mg^{-1}.min^{-1}$) model. Thus, the plot of t/Q_{et} versus t gives straight line whose its slope and intercept are equal to $1/Q_e$ and $1/Q_e^2 k_2$, respectively.

The initial sorption rate h ($mg.g^{-1}.min^{-1}$) was calculated when t approximates to zero as follows equation (7):

$$h = k_2 Q_e^2 \quad (7)$$

Then the equation (6) becomes equation (8):

$$\frac{t}{Q_{et}} = \frac{1}{h} + \frac{1}{Q_e} t \quad (8)$$

2.9 Isotherm Adsorption Modelling

The adsorption equilibrium data were tailored by three isotherm models including Langmuir, Freundlich, Dubinin–Radushkevich (D–R) to describe the adsorbent-adsorbate equilibrium in aqueous system. The laws governing the adsorption of solutes derived from the Gibbs [21] equation (9):

$$\Gamma = -\frac{C}{RT}\left(\frac{d\delta}{dC}\right) \quad (9)$$

where Γ is the number of molecules attached per unit area, C is the average concentration of solute and $d\delta$ is changes in surface tension of solvent depending on the concentration of solute. Integration at constant temperature, the differential relation Gibbs led the laws isothermal Langmuir and Freundlich.

Langmuir adsorption isotherm is based on the assumption that only one monolayer is formed during reaction, presence of equivalent sites, immobility of adsorbate and absence of adsorbate-adsorbent interaction. The linear form of Langmuir equation, equation (10) is the following [21]:

$$\frac{C_e}{Q_e} = \frac{C_e}{Q_m} + \frac{1}{K_L Q_m} \quad (10)$$

where C_e is the equilibrium concentration of the studied metal (mg/L) and Q_e is the amount of the metal adsorbed per gram of adsorbent (mg/g). Q and K_L are Langmuir constant relating the adsorption capacity (mg/g) and the energy of adsorption (L/g), respectively. These constants can be calculated from the slope and intercept of the linear plots of C_e/Q_e versus C_e, respectively. A dimensionless constant called equilibrium parameter R_L that is defined by the following equation (11):

$$R_L = \frac{1}{\left(1 + K_L C_0\right)} \quad (11)$$

where C_0 is the initial concentration of the dye. Depending on the R_L value, there is four possibilities for adsorption: (i) unfavorable (RL>1), (ii) linear (RL = 1), (iii) favorable (0<RL<1), or (iv) irreversible (RL = 0).

The adsorption data were also analyzed with Freundlich isotherm which expressed the adsorption on heterogeneous surfaces of solid with infinity site. The logarithmic form of the Freundlich equation (12) [22] is:

$$\ln Q_e = \ln K_F + n \ln C_e \quad (12)$$

where K_F (L/mg) and 1/n are Freundlich constants. The adsorption process to be linear (n = 1), chemical (n < 1) and favorable physical process (n > 1). Therefore K_F and $1/n$ were determined from the intercept and the slop of the linear plot of ln Q_e against ln C_e.

The Dubinin-Radushkevich isotherm (D-R) was applied to the adsorption data to determine the predominant type adsorption. The linear form of this model is described by the following equation (13) [23]:

$$\ln Q_e = \ln Q_m - \beta \varepsilon^2 \quad (13)$$

where ε is the Polanyi potential equation (14)

$$\varepsilon = RT \ln\left(1 + \frac{1}{C_e}\right) \quad (14)$$

where R is the universal gas constant (8.314 J/mol.K), T (K) is the absolute temperature and β ± (mg^2/kJ) is a constant linked to the adsorption energy. The values of Q_m and β are calculated from the intercept and slope of the plot ln Q_e against ε^2. The average adsorption energy E (kJ/mol) is determined from the following equation (15).

$$E = \frac{1}{\sqrt{-2\beta}} \quad (15)$$

The withdrawal mechanism occurs mainly (i) via physical interaction when E < 8 kJ/mol and (ii) by ion exchange if 8 kJ/mol ≤ E ≤ 16 kJ/mol [23].

3. Results and Discussions

3.1 Characterization of the Powder

Cation exchange capacity (CEC) is one of the crucial means for assessing the general chemical properties of clays. Table 1 presents

the estimated CEC values for the raw (RM) and treated (TM) clay samples along with these reported for different materials in the literature. The CEC of TM clay is slightly significant (51 meq/100g) than that of RM sample due to high availability of active materials and the effectiveness of the purification process.

Surface acidity of clay minerals describes their ability to donate a proton or an electron pair. Usually, it is expressed in terms of Bronsted acid sites (donate protons) and Lewis acid sites (accept electron) which are represented by different surface groups and ions (exchangeable cations. Coordinatively unsaturated ions Al^{3+}, Mg^{2+}, Fe^{3+}, acid/basic hydroxyl groups and oxygen anions). The nature of surface sites of RM clay sample are determined by using potentiometric titration. As reported in Table 2, the surface of RM clay is positively charged in the whole range of pH acid. The weak isomorphic substitution of low valence cations for higher valence cations and the influence of the contaminant minerals such as kaolinite and illite are expected to be the primarily reasons of elevated yield of acidic products. It is wealthy to know that kaolinite and illite, which are alumino-silicate clays, have the higher Lewis acid components. Besides, Brønsted acid sites are characterized by M^{VI}–OH (M = Si, Al, Mg, Fe), in agreement

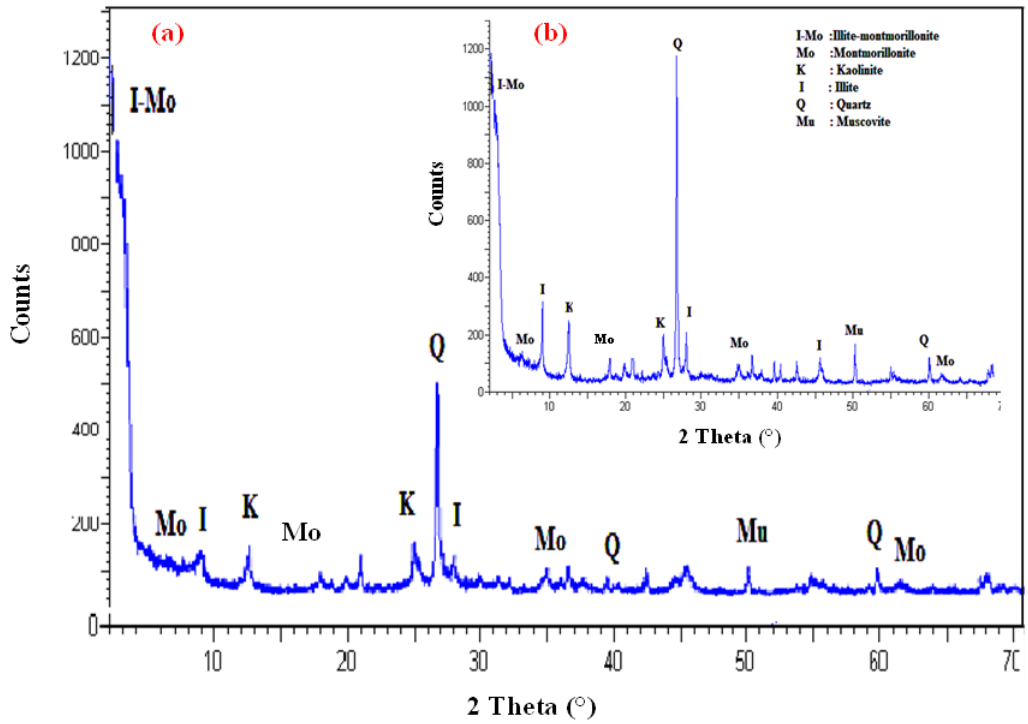

Figure 2. XRD pattern of TM sodium clay monoionique (a). Inset : XRD pattern of RM (b).

Table 1. Cation exchange capacity (CEC) in meq/100g of clay minerals [24]

Minerals	NT clays		K	I	K	OM	S	*LS to SL*	*L*	*C*
	RM	TM								
CEC meq/100g	35–50	51	3–15	15–40	80–100	200–400	1–5	5–10	5–15	>30

NT clays: Naima-Tiaret Clays; K: kaolinite; I: Illite; M: Montmorillonite; OM: Organic matter; S: Sand; *LS to SL: Loamy Sand to Sandy Loam; L: Loam and C: Clay*

Table 2. The surface acidity of RM clay.

pH	5.45	5.55	5.59	5.62	5.83	5.90	6.2	7.5
Surface acidity	Q > 0	Q > 0	Q > 0	Q > 0	Q > 0	Q > 0	Q > 0	n.d

n.d.: not detected

with FT–IR results which revealed an intense band at 1600 – 1400 cm^{-1} region.

The XRD patterns of the raw (RM) and treated (TM) clay samples are displayed in Figure 2. XRD patterns of the both clay samples displayed mainly basal reflections of montmorillonitic, illite with interstratified illite-montmorillonite, quartz and kaolinite as the major phase, besides minor amounts of muscovite (mica derivative group) and chlorite minerals. In the XRD patterns of raw clay (RM), montmorillonite was identified by the presence of peak (001) at 2θ = 6.49° and (003) at 2θ = 17.17° while illite was evidenced by the main peak (002) at 2θ = 8.87°. The basal spacing at 7.20 Å and 3.58 Å corresponding to the (0 0 1) and (0 0 2) reflections, confirming the presence of kaolinite. The interstratified illite-montmorillonite (interstratified I/M) was evidenced by the main peak located at 2θ = 3.42 ° with a calculated basal spacing of 25.83 Å. Additionally, quartz was presented by the prominent peak (011) at 3.33 Å. In the sodium clay monoionique (TM) sample, no significant change in the XRD profile was observed upon purification process. However, the decrease in intensity of the quartz reflections at 2θ = 27.8° (3.2 Å), indicating effectiveness of the purification process [25].

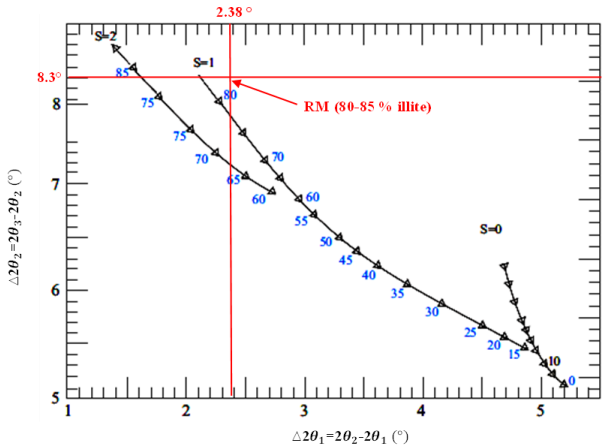

Figure 3. Diagram for identification of interstratified illite/ montmorillonite ($\Delta 2\theta_1$ and $\Delta 2\theta_2$ value on the diagram represents the value of the difference in the angle of reflection (Cu K_α radiation) [26].

Interstratified montmorillonite / illite (denoted as Interstratified I/M) is a two-component mixed-layer minerals composed of dioctahedral illite and montmorillonite. Mixed-layer minerals are identified as components, proportions, and levels of composition order that has been determined. As a parable, the mixed-layer minerals consisting of two components A-B. The two components are probabilities and be grouped into types of Random Sequence Stacking (S=0): Random Sequence Stacking (S=0) is a sequence of random stacking, la yer A can be followed by A or B layer without provisions sequence. Maximum Degree of Order (S=1): While the Maximum Degree of Order (S=1) is a sequence of layers with the provisions of the order, for example, when a layer of clay mineral composition of sequences is composed of 10 layers containing 40% B, hence the sequence arrangement applied as follows: B-A-B-A-A-B-A-B-A-A. The sequence may be present, but when the order as B-A-A-AB-B-A-B-A-A, then it is not allowed. A long-range order (S>1): can be formed with at least two or three in a row A after each B. Thus the interstratified illite/montmorillonite has a layer variation between illite/montmorillonite.

The determination of the type and percentage of interstratified I/M was based on the calculation method of Watanabe [26]. This first calculating can be traced as follows: $2\theta_2 - 2\theta_1 = \Delta 2\theta_1$ and $2\theta_3 - 2\theta_2 = \Delta 2\theta_2$. The results of these calculations will result in $\Delta 2\theta_2$ and $\Delta 2\theta_1$ values. Calculation results of $\Delta 2\theta_2$ and $\Delta 2\theta_1$ are then plotted on the diagram variation $\Delta 2\theta_2$ and $\Delta 2\theta_1$, so the values of the proportion of interstratified illite/montmorillonite will be obtained. The calculation results of the type and percentage of interstratified I/M in the RM sample only are presented in Table 3. Plotting of the results can be seen in Figure 3. From the result of variation diagram diagram $\Delta 2\theta_1$ and $\Delta 2\theta_2$ plotting, the obtained values of S = 1 varies from 80 – 85% illite.

Chemical analysis showed that silica (SiO_2), alumina (Al_2O_3) and ferric oxide (Fe_2O_3) are the three main components of RM and TM clays, as summarized in Table 4. Besides, the RM clay collected in the NAIMA region, contained calci-

Table 3. Calculation results interstratified Illite/Montmorillonite using calculation methods of Watanabe show type interstratified S = 1 and % illite.

Clay soils	$2\theta_1$ (°)	$d_{(hkl)}$ (Å)	$2\theta_2$ (°)	$d_{(hkl)}$ (Å)	$2\theta_3$ (°)	$d_{(hkl)}$ (Å)	$\Delta 2\theta_1=2\theta_2-2\theta_1$ (°)	$\Delta 2\theta_2=2\theta_3-2\theta_2$ (°)	S=1	Illite (%)
RM	6.49	13.61	8.87	9.96	17.17	5.16	2.38	8.3	80–85	80–85

um, potassium, magnesium and titanium oxides, as obvious minor amounts, with other metal cations, traces fractions. The mass fraction of silica and alumina increased from 42.2 to 46.45% and from 11.97 to 12.98%, respectively. Conversely, the CaO and MgO mass fraction decreased from 1.52 to 1.23% and from 2.05 to 1.97%, respectively. The magnesium oxide content in both samples can give evidence to the presence of smectite [12]. Furthermore, the occurrence of these oxides suggested the presence of mineral contaminants such as dolomite [$CaMg(CO_3)_2$] and calcite ($CaCO_3$). It should be highlighted that the contents of SiO_2 and Al_2O_3 were apparently higher in TM as compared to these in RM clay. The removal of carbonate and organic matter improved by the percentage of silica and alumina in the treated clay, nevertheless the exchangeable and octahedral cations clearly decreased, which are in good consistency with the reported studies [27]. The SiO_2/Al_2O_3 molar ratio of 3.52 and 3.57 for RM and TM, respectively are greater than those of ideal kaolinite (1.18) [28] and montmorillonite (2.36), suggesting the occurrence of quartz and other silicates in both clay samples compared to the aluminum probably due to the detritus load of the neighboring continental area [29]. The prominent K_2O content may indicate the possible presence of large amounts of illite in both samples [30], as displayed in Table 3. Based on the chemical properties, the clay samples explored are expected to demonstrate distinct removal profile. The presence of carbonate contents in both clays can improve the removal of Cu^{2+} and Zn^{2+} metal ions in adsorption process. It is likely that RM clay can remove higher amounts of metal ions than the TM sample. Such a composition would contribute to higher removal of Cu^{2+} and Zn^{2+} metal ions due to the presence of aluminol (Al–O) and silanol (Si–O) groups) on the surface of the clay samples studied.

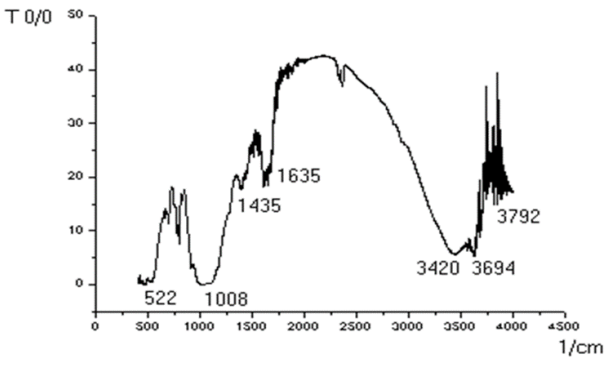

Figure 4. FT-IR spectrum of TM clay sample.

Figure 4 illustrates the FT–IR spectrum of the treated clay (TM). From the FT–IR spectrum obtained, the following minerals were classified: *OH group* indicated by two adsorption bands ranges between 3200–3800 cm^{-1} and between 1600–1700 cm^{-1}. The band near 1600–1700 cm^{-1} is attributed to the bending vibration of adsorbed hydroxyl groups of water. Bands in the range 3200–3800 cm^{-1} with an intense band and landslide in 3625 and 3400 cm^{-1} characteristic of montmorillonite related to stretching vibrations of OH groups of the octahedral coordinated either 1AL + 1Mg (3640 cm^{-1}) or 2Al (3620 cm^{-1}). The bending vibrations of H_2O molecules are characterized by the band at 3400 cm^{-1}. The band located around 1630 cm^{-1} is ascribed to deformation vibrations of adsorbed H_2O molecules between the sheets. *Si–O group*: the Si–O are characterized by the intense band between 900–1200 cm^{-1} and centred around 1040 cm^{-1} are attributed to the stretching vibrations of the Si–O. The lower wavenumbers at 525, 468 and 425 cm^{-1} indica-

Table 4. Physico-chemical properties of the studied clay samples (wt%).

Elements	Raw clay (RM) (wt%)	Treated clay (TM) (wt%)
SiO_2	42.21	46.45
Al_2O_3	11.97	12.98
Fe_2O_3	5.8	5.48
K_2O	3.32	3.45
MgO	2.05	1.97
CaO	1.52	1.23
TiO_2	0.84	0.89
Ba	0.05	0.04
P_2O_5	0.04	nd
Rb	0.03	0.02
MnO	0.02	0.03
Sr	0.02	0.01
V	0.01	0.01
Zr	0.01	0.01
Cl	0.01	nd
Ta	0.009	nd
Y	0.006	0.006
Ag	0.005	nd
Cu	0.004	0.007
Ni	0.003	nd
Mo	0.002	nd
As	0.001	nd

nd : not detected

tive of a greater proportion of Si–O–Al^{VI}, Si–O–Mg^{VI} and Si–O–Fe in the clays. *M^{VI}–OH (M= Al, Mg, Fe) bonds* or *illite-montmorillonite*. The sharing of the OH group between the atoms Fe and Al in octahedral position may move Al–OH vibrations at low frequencies around 815 and 915 cm^{-1}. Thus the vibration Mg–O and Mg–OH (combined with that of Si–O) located at 530 and 560 cm^{-1}, respectively [31–35], highlighted the presence of illite-montmorillonite mixtures. Kaolinite: the intense band at 3694 cm^{-1} corroborated the presence of kaolinite [36]. *Quartz*: *quartz* usually detected by two characteristic bands near 790–795 cm^{-1} and 750–755 cm^{-1}. *Calcite*: the stretching band at 1435 cm^{-1}, corresponded to the CO stretching of carbonate, is attributed to calcite.

The impact of the temperature on electrical conductivity of our clays used in this study is reported in Figure 5. The electrical conductivity of the both clays showed different sensitivities to temperature. For TM sample, the electrical conductivity sharply increased from 8.9×10^{-7} Ω^{-1} m^{-1} at 8 °C to 1.45×10^{-6} Ω^{-1} m^{-1} at 32 °C and decreased linearly with rising temperature, almost reaching 2.23×10^{-7} Ω^{-1} m^{-1} at 140 °C. For the pristine RM clay, the electrical conductivity slightly increased from 2.12×10^{-7} to 1.69×10^{-6} Ω^{-1} m^{-1} as the temperature was increased from 8 to 100 °C and then declined severely to 9.13×10^{-8} Ω^{-1} m^{-1} at 140 °C. For low temperature (8 °C ≤ T ≤72 °C), significant electrical conductivity ($\sigma = 1.45\times10^{-6}$ Ω^{-1} m^{-1}) for TM clay was observed, whereas a significant conductivity response ($\sigma = 1.69\times10^{-6}$ Ω^{-1} m^{-1}) for RM sample as found for high temperature (72 °C ≤ T ≤ 140 °C). Higher electrical conductivity is associated with moisture content and saturation of clay, and this is presented by

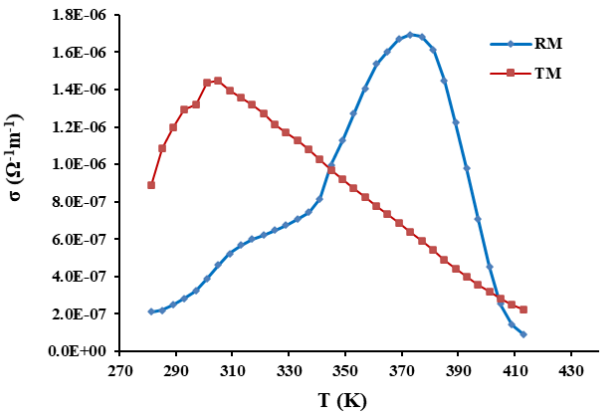

Figure 5. Conductivity measurement of RM and TM clay samples.

many researchers [37]. However, there are many parameters that can affect the measurement of the electric conductivity such as clay texture, porosity, particle-size distribution, mineralogical composition, form and distribution of water in clay, salt content, charge carriers and temperature. An increase in temperature can result in a rise in clay electrical conductivity. The mobility of Na^+ counter-ions and the charge carriers are the main driving force for increasing the electrical conductivity for TM clay. However, the reduction in conductivity with temperature being due to a smaller proportion of these ions in the Gouy layer and/or a decrease in their mobilities. For the pristine RM clay, in contrast, the optimum moisture content (saturation) is found to be the primarly cause for rising the electrical conductivity, while, the decline in electrical conductivity with temperature is ascribed tothe decrease in the mobility of the charge carriers and the moisture exclusion effect (via drainage and evaporation process).

The SEM images of the clay samples with different resolutions are shown in the Figure 6. The SEM image of the bare RM (Figures 6 (a-c)), collected in the Naima region, revealed a uniform paste with a few dolomite rhombohedra. The sample showed lamellar flakes and a spongy structure, which could be a typical SEM micrograph of sodium montmorillonite [38]. In contrast to the RM sample, the TM clay particles are in the form of clusters of fine aggregates and platelets in the form of sticks with irregular contours, as displayed in Figure 6 (d-g). This is a morphology encountered both for poorly crystallized kaolinites and illite as observed by Konan [39]. The SEM image shown in Figure 6 (b) and in agreement with what we obtained in XRD analysis. There is no doubt about the presence of carbonates and quartz in the sample. Carbonates and calcite are in the form of clearly visible aggregates and quartz is in the form of small grains [40].

The energy dispersive X-ray (EDX) mapping was carried out to determine the chemical composition of the clay samples. The EDX spectrum shown in Figure 7, obviously reveals the presence of Si, Al, Mg, Fe, K, P, S, O, Ca, C elements within the RM clay sample (Table 5). There is a significantly high concentration of silicon mainly due to the majority presence of quartz in the sample studied. These results are in good accordance with XRF and XRD analysis which revealed the occurrence of these elements in the form of oxides, such as: Al_2O_3, SiO_2, Fe_2O_3, MgO, $CaCO_3$, and K_2O. Mean-

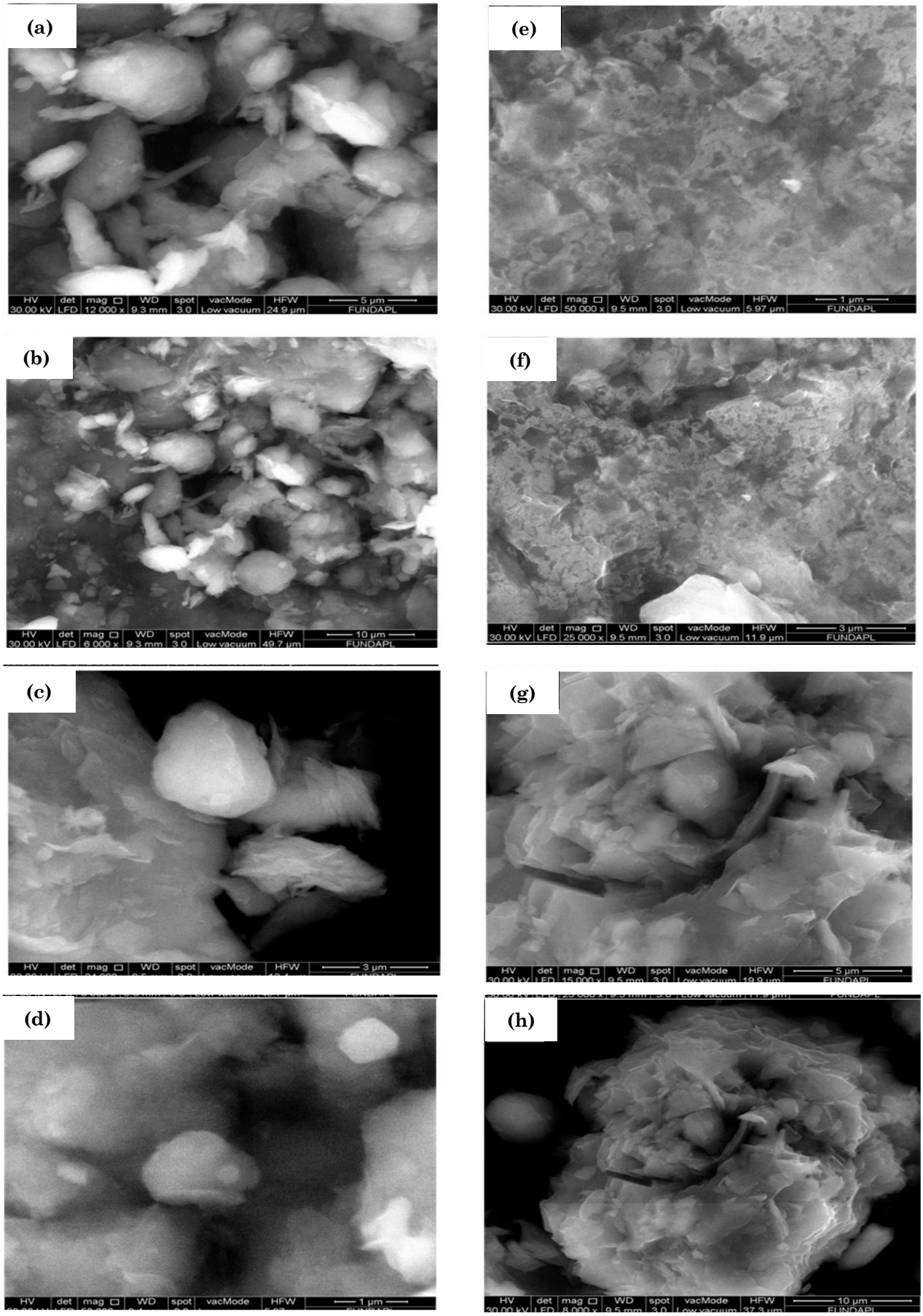

Figure 6. SEM images of clay soils: (a-**d)** RM clay and (e-h) TM clay samples.

while, the appearance of new peaks corresponding to the carbon element, probably coming from the support grid of the sample. The EDX result largely confirms the presence of the clay phases in relation to the percentage of silicon, aluminum and oxygen. Carbon ions are absent in the spectrum of TM clay (Figure 8) and the results basically confirm the removal of carbonate and organic matter during treatment process. The low potassium fraction and the absence of calcium in the treated clay indicates the efficient exchange of these ions by the sodium species which makes the clay surface more homogeneous, so in this case we are talking about a sodium mono ionic clay. The discrepancy observed between the total net and normal composition for both clay soils attributed to the loss of the precursor powders during synthesis route. As displayed in Table 5, the total net composition for RM (102.42 wt%) and for TM (154.41 wt%) appeared higher than normal composition (100.00 wt%).

3.2 Adsorption Experience

3.2.1 Effect of contact time

The impact of contact time on the adsorption of Zn^{2+} and Cu^{2+} metal ions on the RM and TM clays was investigated and the results were displayed in Figure 9. Basically, the adsorption process of these ions was fast in the first 10 min with more than 95% of the total adsorption capacity obtained for the both Zn^{2+} and Cu^{2+} ions, and then gradually slows until equilibrium sorption metal/clay was reached after 60 min. The sorption capacity of clay

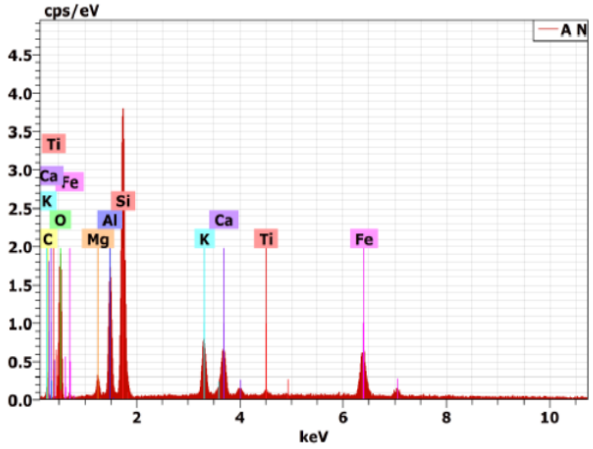

Figure 7. EDX spectrum of RM clay sample.

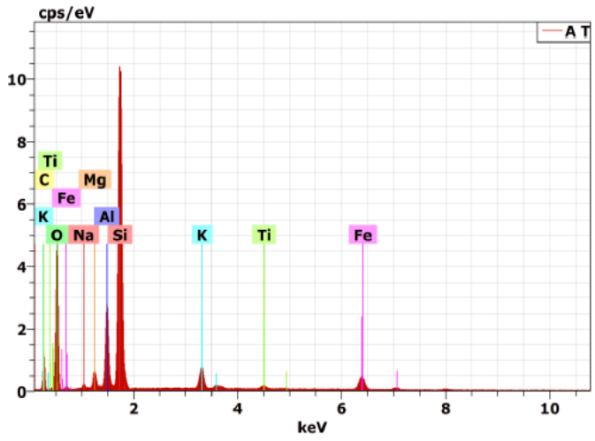

Figure 8. EDX spectrum of TM clay sample.

Table 5. Energy dispersive X-ray test results of the clay samples.

Elements	RM composition		TM composition	
	Net (wt%)	Normal (wt%)	Net (wt%)	Normal (wt%)
Silicium (Si)	19.75	19.29	27.62	17.89
Oxygen (O)	47.95	46.81	75.90	49.16
Aluminium (Al)	7.56	7.39	7.60	4.92
Potassium (K)	3.68	3.59	1.90	1.23
Iron (Fe)	3.48	3.39	2.30	1.49
Carbon (C)	14.76	14.42	35.35	22.89
Magnesium (Mg)	1.29	1.26	2.24	1.45
Titanium (Ti)	0.39	0.39	0.45	0.29
Sodium (Na)	nd	Nd	1.05	0.68
Total (wt%)	102.42	100.00	154.41	100.00
Error (wt%)	2.42		54.41	

nd : not detected

samples towards Cu^{2+} and Zn^{2+} ions were 4.53 and 2.07 mg/g for RM and 3.45 and 2.15 mg/g for TM clay, respectively. The adsorption of Cu^{2+} was approximately 2 times higher than that of Zn^{2+} for RM and almost 1.5 time as much as that of Zn^{2+} for TM clay.

The enhanced sorption efficiency of Zn^{2+} and Cu^{2+} metal ions in the first adsorption stage was primarily attributed to the precipitation as copper and zinc carbonates, in consistency with XRF, FT−IR, EDS and mineralogical composition analysis which reveal the occurrence of carbonate minerals. However, in the second stage, subsequent gradual adsorption may be attributed to the saturation and removal of carbonate minerals. So, on the base of the kinetic results, the adsorption equilibrium time of 60 min was chosen as a compromise between theory and practical approach [41]. The discrepancy in removal capacity of clay soils (RM and TM) toward heavy metal ions at the same operating conditions may be ascribed in point of view mineralogical composition feature (high CaO and MgO contents and low K_2O mass fraction in RM compared to these of TM), determination of the type and percentage of interstratified I/M aspect (less proportion of interstratified I/M type S=1 (less % of illite) in the RM in comparison to TM, acting as a passive phase) and molecular size of the adsorbed metal ions (ionic radii of Cu^{2+} ion (72 pm) is lower than Zn^{2+} (74 pm)). This allows probably to remove higher amounts of Cu^{2+} metal ions than Zn^{2+} ions and greater adsorption capacity of RM for Cu^{2+} ion than TM, via ion-exchange process.

The adsorptions of Cu^{2+} and Zn^{2+} metal ions on RM and TM clays were studied kinetically using pseudo-first order and pseudo-second order models. Kinetic parameters of the pseudo-first-order and pseudo-second-order models for the adsorption of Cu^{2+} and Zn^{2+} metal ions on RM and TM clays are presented in Table 6. As it can be seen, the straight lines for the entire RM and TM clays of the plots of t/Q_{et} versus t (Figures 10a-b), with high regression coefficients (R^2 = 0.968−0.999) strongly suggest that the sorption processes of Cu^{2+} and Zn^{2+} ions on the both clays were satisfactorily fitted the pseudo-first-order model. Moreover, the calculated Q_e values are almost closer to the experimental data, indicating that the adsorption processes are controlled by a chemical adsorp-

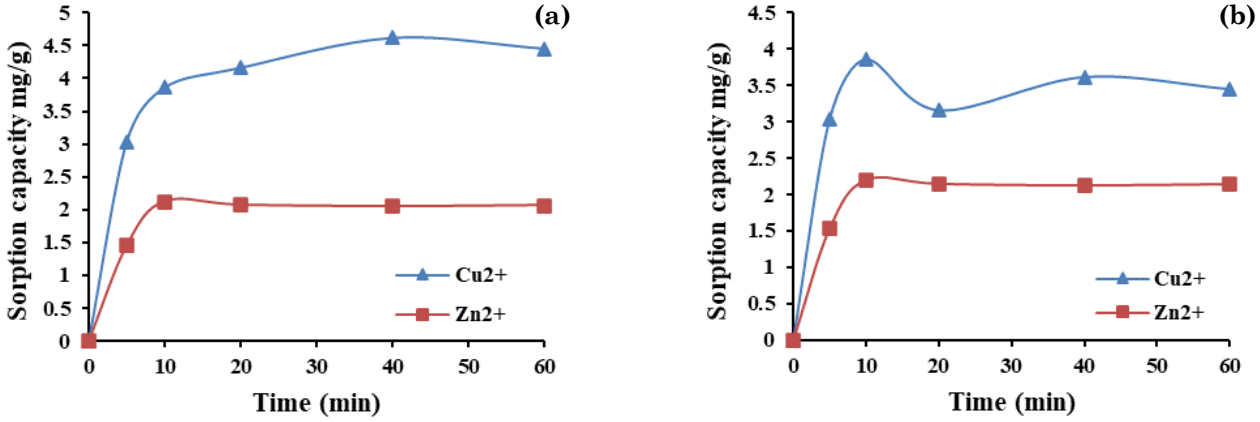

Figure 9. Effect of contact time on Cu^{2+} and Zn^{2+} adsorption onto **(a)** RM and **(b)** TM clay samples

Table 6. Pseudo first and second order kinetic parameters for the sorption of Cu^{2+} and Zn^{2+} ions onto RM and TM clays.

Clays abbr.	Metal ions	Exp. results Q_{exp} (mg/g)	Pseudo-first-order model			Pseudo-second-order model			
			Q_{cal} (mg/g)	k_1 (1/min)	R^2	Q_{cal} (mg/g)	k_2 (g/mg.min)	h (mg g^{-1} min^{-1})	R^2
RM	Cu^{2+}	4.53	1.239	0.043	0.758	4.69	0.094	2.075	0.998
	Zn^{2+}	2.07	1.136	0.002	0.08	2.50	0.143	0.897	0.968
TM	Cu^{2+}	3.45	1.397	0.001	0.002	3.49	1.185	14.430	0.997
	Zn^{2+}	2.15	1.433	0.004	0.21	2.16	0.834	3.891	0.999

abbr.: Abbreviation; Exp.: Experimental

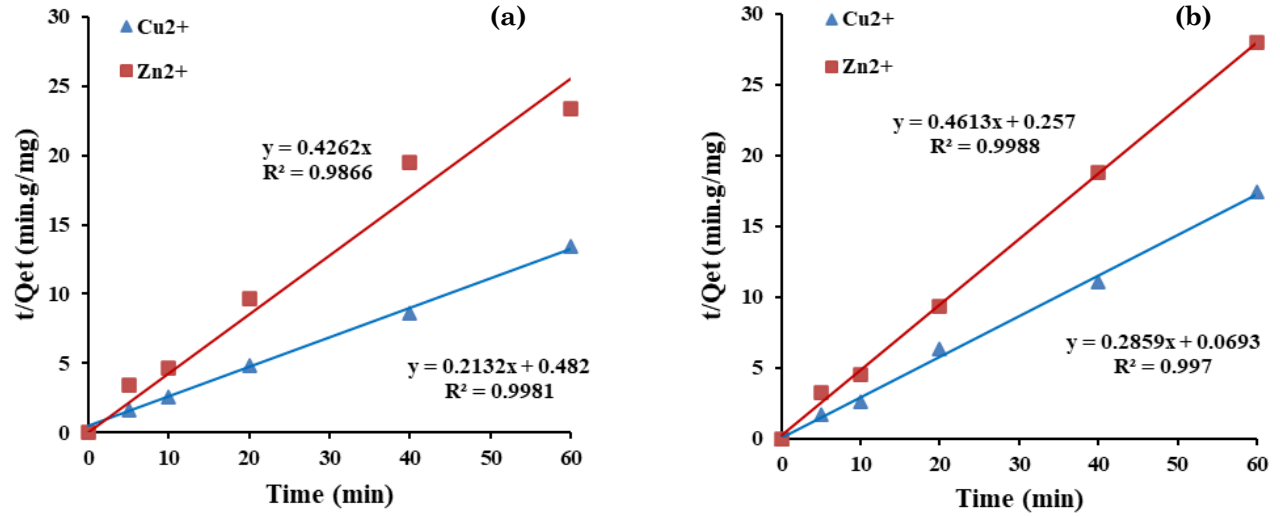

Figure 10. Pseudo-second order kinetic of the Cu^{2+} and Zn^{2+} adsorption onto **(a)** RM and **(b)** TM clay samples.

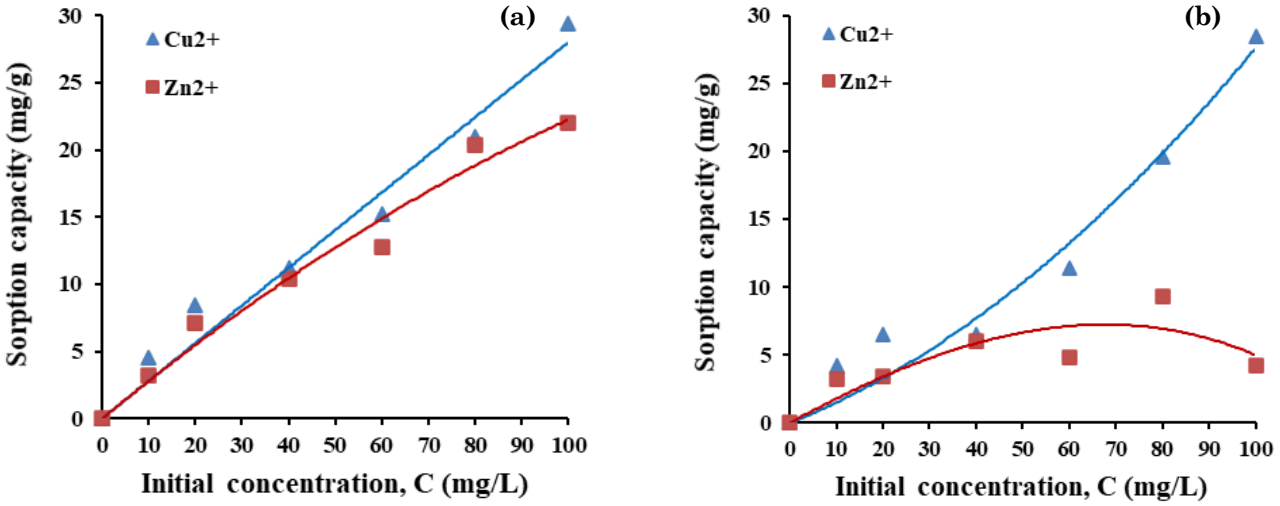

Figure 11. Effect of initial concentration on Cu^{2+} and Zn^{2+} adsorption onto **(a)** RM and **(b)** TM clay samples

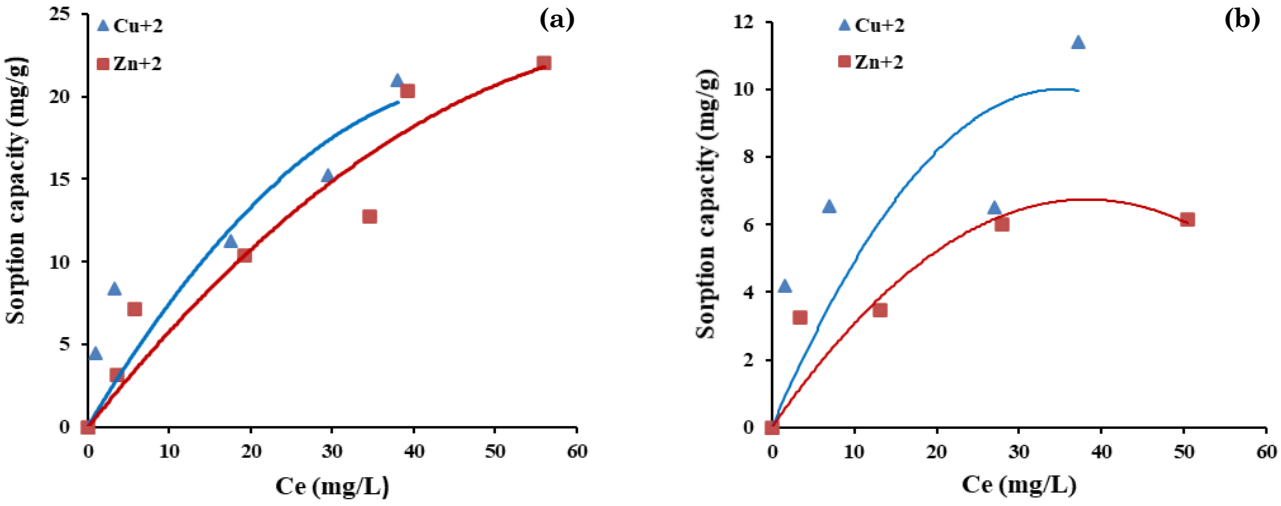

Figure 12. Adsorption isotherms of Cu^{2+} and Zn^{2+}ions onto **(a)** RM and **(b)** TM clay samples.

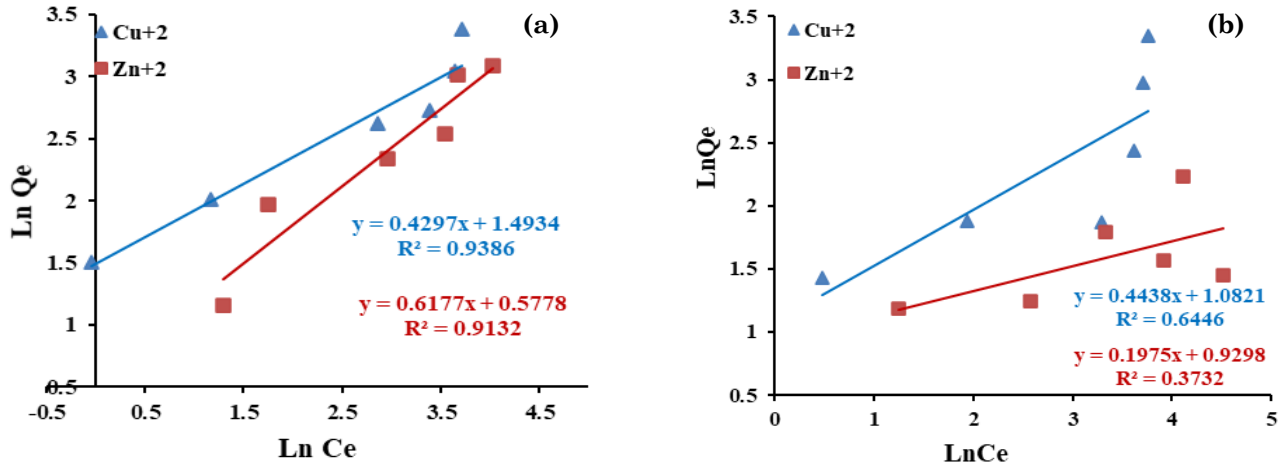

Figure 13. Freundlich isotherms: **(a)** RM and **(b)** TM clay samples.

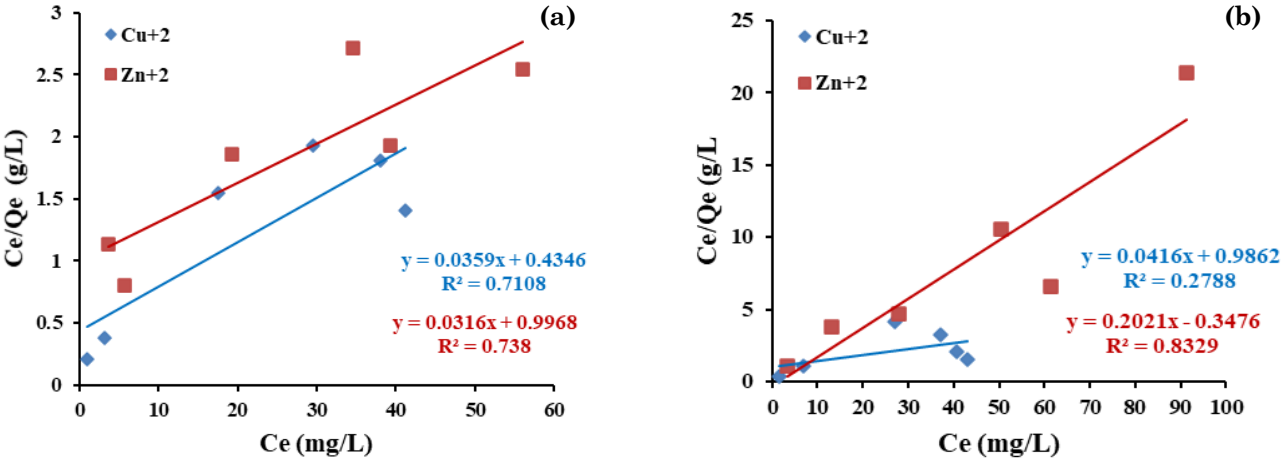

Figure 14. Langmuir isotherms: **(a)** RM and **(b)** TM clay samples

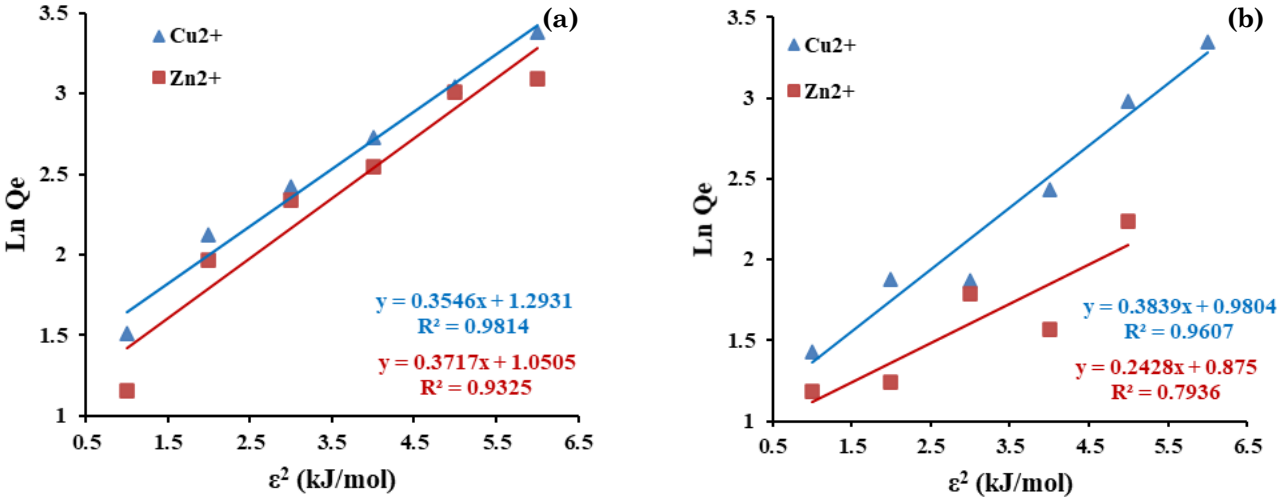

Figure 15. Dubinin-Radushkevich 'DR isotherms: **(a)** RM and **(b)** TM clay samples.

tion process. On the other hand, the pseudo-first-order model ($R^2 < 0.758$) is not a suitable model for describing the adsorption kinetics for the both dyes onto clays. The calculated and experimental values Q_e diverged significantly, as summarized in Table 6.

3.2.2 Influence of initial concentration

The effect of the concentration on the adsorption of Cu^{2+} and Zn^{2+} metal ions were conducted at various initial concentrations of 10, 20, 40, 60, 80 and 100 mg/L at room temperature and pH of 5.7 within the equilibrium time of 60 min. As illustrated in Figure 11, the sorption capacity of the RM (Figure 11(a)) and TM (Figure 11(b)) clays towards Cu^{2+} ions linearly increased with increasing initial concentrations until the saturation of the available adsorption site, and 29.37 and 28.47 mg/g were obtained, respectively. For the same optimum contact time of 60 min, a similar tendency was observed for Zn^{2+} ions removal by RM clay (Figure 11(a)) with a maximum of 22.00 mg/g. Conversely, the sorption capacity of TM clay for Zn^{2+} ions gradually increased with rising contact time, and then remained almost constant after equilibrium, as displayed in Figure 11(b).

The maximum sorption capacity of TM clay for Zn^{2+} ions was found to be 6.10 mg/g. On the base of the above results, the bare NAIMA RM clay demonstrated high effectiveness in adsorbing of metal ions such as Zn^{2+} and Cu^{2+}, hence the sequential sorption capacity was as follow:

$Cu^{2+}{}_{(RM)n} > Cu^{2+}{}_{(TM)} > Zn^{2+}{}_{(RM)} > Zn^{2+}{}_{(TM)}$.

3.2.3 Adsorption isotherms

Figure 12 described the equilibrium adsorption curves of Cu^{2+} and Zn^{2+} ions onto clay samples at room temperature. The adsorption of the both metal ions (Cu^{2+} and Zn^{2+}) forms a typical Freundlich isotherm-type on the both clays, according to Giles classification system [42]. The maximum adsorption capacity of RM and TM clays were found to be 20.98 and 22.00 mg/g for Cu^{2+} ions, and 11.42 and 6.13 mg/g for Zn^{2+}, respectively.

The adsorption equilibrium data were tailored by three isotherm models including Langmuir, Freundlich, Dubinin–Radushkevich (D–R). The linearized Freundlich, Langmuir and Dubinin-Radushkevich 'DR adsorption isotherms of each clay sample for Cu^{2+} and Zn^{2+} ions are displayed in Figures 13a-b, 14a-b, 15a-b, respectively, and their model parameters are listed in Table 7. On the base of the regression coefficients (R^2) of the linearized form of the D-R adsorption isotherm (0.794 − 0.981), we believe this isotherm model more suitable with this adsorption process than Freundlich and Langmuir models. In addition, the adsorption energy (E) given by D-R model suggests the ion exchange nature of the retention mechanism in most cases (E > 8 kJ / mol). The adsorption energy (E) for Cu ions (12.909 kJ/mol) are higher than that of Zn ions (11.18 kJ/mol), implying that Cu ions are more active and dynamic in the adsorption process, especially on RM. Furthermore, the values of Freundlich constant K_F was higher for adsorption of Cu^{2+} ions on RM clay as compared to the adsorption on TM clay. All the n-values for the adsorption of Cu^{2+} and Zn^{2+} ions on clays are in the range of 0–1 ($0 < n < 1$), suggesting that the adsorption process is favorable. The separation factor R_L varied between 0 and 1, confirming a favorable adsorption under the experimental conditions of the study. It is obviously seen that the maximum adsorbed capacity Q_m (mg/g) deduced from Langmuir and D–R models, respectively, were not comparable in most cases, and were significantly lower than the experimental results. So, we can conclude that the best fit to D-R model due to the high

Table 7. Adsorption isotherm parameters for Freundlich, Langmuir and Dubinin-Radushkevich (D-R) models.

Clays abbr.	Exp. results		Freundlich model			Langmuir model				Dubinin-Radushkevich (D-R) model			
	Metal ions	Q_{exp} (mg/g)	K_F (L/g)	n	R^2	Q_m (mg/g)	K_L (L/mg)	R_L	R^2	Q (mg/g)	β (mol²/kJ²)	E (kJ/mol)	R^2
RM	Cu^{2+}	20.98	4.452	0.429	0.939	28.57	0.073	0.43	0.711	19.638	0.003	12.909	0.981
	Zn^{2+}	22.00	1.782	0.618	0.913	32.25	0.036	0.99	0.738	11.233	0.004	11.18	0.932
TM	Cu^{2+}	11.42	2.951	0.444	0.645	24.39	0.042	0.99	0.279	9.559	0.004	11.18	0.961
	Zn^{2+}	6.13	2.534	0.197	0.373	4.95	0.581	0.34	0.833	7.499	0.002	15.811	0.794

abbr.: Abbreviation; Exp.: Experimental

correlation coefficient (R^2) [43,44].

3.2.4 Potential adsorption mechanisms

In the interstratified illite/montmorillonite (interstratified I/M), illite and montmorillonite both consist of aluminosilicate layers alternating with interlayers. In illite layers, the interlayer cations is prominently potassium (K^+) ions. These are non-hydrated, due to how they are 'fixed' in the ditrigonal cavities on the surfaces of the tetrahedral sheet. As a result of the non-hydrated nature of its interlayer cations, it is a non-swelling clay mineral, in contrast to some montmorillonites. However, the interlayer cation in the montmorillonite layers, predominately sodium (Na^+), have the capacity to be become hydrated – the formation of diffuse double layers via osmosis results in swelling behavior [45]. The exchangeable interlayer Na^+ cations (ionic radii of Na^+ ion is 97 pm) can be exchanged with other ions, Cu^{2+} (ionic radii of Cu^{2+} is 72 pm) or Zn (ionic radii of Zn^{2+} is 74 pm)) metal ions in our assays, relatively easily via ion exchange mechanism without affecting the clay mineral structure. Further, in acidic environments, the release of H^+ ions from the edge (more active) of structure causes metal adsorption, from aqueous matrices, onto the edges of TM or RM samples for ions like Cu^{2+} or Zn^{2+}. Figure 16 shows the schematic diagram of the ion exchange mechanism of Cu^{2+} or Zn^{2+} metal ions on the surface of TM or RM interstratified I/M clay soils.

3.4.5 Comparison with other studies

Based on previous relevant studies, the amount of heavy metals removed by various clay materials is highly variable, as displayed in Table 8. In the current study, natural clay samples have demonstrated significant elimination of metals compared to the treated forms. It was clear from the study data that the efficiency of elimination depended on the physicochemical characteristics of clay and metal. The calculated capacities of Langmuir (RM and TM) were 28.57 and 24.39 mg/g for copper, 32.25 and 4.95 mg/g for Zinc. In general, the removal remained more or less con-

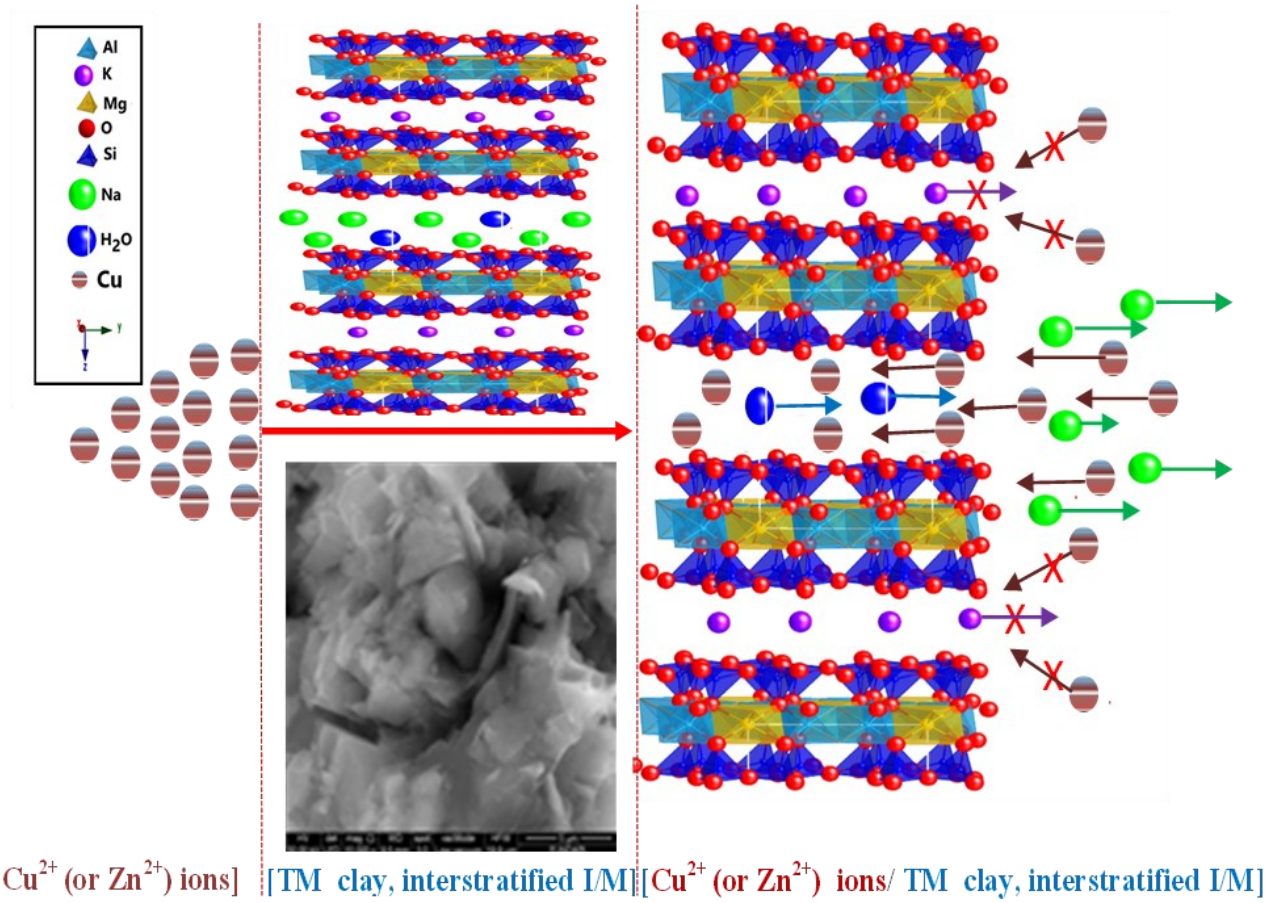

Figure 16. The ion exchange mechanism of Cu^{2+} or Zn^{2+} metal ions on the surface of TM or RM interstratified I/M clay soils.

stant in the case of RM and TM for copper and decreased for zinc. All these results indicate a much higher elimination efficiency of the clay samples present than those shown by Bhattacharyya and Gupta [46,47] who examined the elimination of metals by various types of clay. We found that the clay samples taken in the Naima region had greater elimination efficiency greater than that reported in the literature. It is therefore possible to confirm that the clays of the Naima region are suitable for the removal of Cu(II) and Zn(II) metal ions from aqueous solution [48−52].

4. Conclusion

Highly efficient purified clay TM (TM stands for the chemically treated clay) collected from sites in the Naima-Tiaret-Algeria region was applied as potential clay adsorbent for the removal of two metal ions, Cu^{2+} and Zn^{2+} in the simulated aqueous solution. The pristine RM (RM stands for the untreated clay) and its purified phase (TM) were subsequently identified by XRF, XRD, FT−IR, SEM−EDX and DC electrical conductivity techniques. Experimental results revealed that clays, with montmorillonitic, illite, and interstratified illite-montmorillonite (I/M) as major phase, exhibited a basal spacing of 25.83 Å, cation exchange capacity of CEC of 51 meq/100g and high Brønsted acid sites. Based on the calculation method of Watanabe, the type of interstratified I/M in the current studied sites is S = 1 and the percentage of illite type S = 1 is between 80 − 85% illite. The electrical conductivity of the both clays showed different sensitivities to temperature. The adsorption equilibrium was established within 60 min. The sorption capacity of the RM and TM clays towards Cu^{2+} ions linearly increased with increasing initial concentrations. The maximum adsorption capacities of Langmuir were 28.57 and 24.39 mg/g for Cu^{2+} onto RM and TM, respectively, 32.25 mg/g and 4.95 mg/g for Zn^{2+} in the presence of RM and TM, respectively. The high regression coefficients (R^2) of the linearized form of the D-R adsorption isotherm (0.794 − 0.981) implied that D-R isotherm model was more suitable with this adsorption process than Freundlich and Langmuir models. In addition, the adsorption energy (E) given by D-R model suggests the ion exchange nature of the retention mechanism in most cases (E > 8 kJ/mol). Pseudo second-order model best described the kinetics of adsorption process. All the n-values for the adsorption of Cu^{2+} and Zn^{2+} ions on clays are in the range of 0–1 ($0 < n < 1$), suggesting that the adsorption process is favorable. Pseudo second-order model best described the kinetics of adsorption process. Energy of adsorption (E) deduced from D-R isotherm suggests physical adsorption. The ion exchange mechanism between exchangeable interlayer cations (Na) in the interstratified I/M and Cu^{2+} or Zn^{2+} metal ions from aqueous matrix, and electrostatic attraction as initial driving force for Cu^{2+} or Zn^{2+} to bind onto the surfaces of TM or RM interstratified I/M clays in acidic environments are the primarily responsible for the improved adsorption efficiency of the both clay soils. Comparison of the adsorption capacity with those of previous studies on the elimination of Cu^{2+} or Zn^{2+} metal ions was also highlighted. The clay from Naima region had greater elimination efficiency than that reported in the literature. Fi-

Table 8. Comparison of the adsorption capacity with those of previous studies on the elimination of Cu(II) and Zn(II) metal ions from aqueous solution.

Metal Ions	Adsorbent	Q_{max} (mg/g)	K_L (l/mg)	pH	Reference
Cu^{2+}	RM	28.57	0.073	5.7	Present study
	TM	24.39	0.042	5.7	Present study
	Kaolin	4.47	0.15	6	[48]
	Bentonite	7.59	3.78	6	[43]
	Illitic clay	17.98	0.212	5.5	[53]
	Kaolinite	4.3	19.9	6	
	Motmorillonite	25.5	43.7	6	
Zn^{2+}	RM	32.25	0.036	5.7	Present study
	TM	4.95	0.581	5.7	Present study
	Bentonite	8.27	8.271	4	[39]
	Motmorillonite	13.26	13.269	3	[44]

nally, this study represents an important source of information on the predominant local clays in the NAIMA region.

Acknowledgement

The authors would like to express their sincere thanks to the Directorate General for Scientific Research and Technological Development and the Ministry of Higher Education and Scientific Research (Algeria) for their financial support.

References

[1] Kaličanin, B., Todorovska Rašić, M. (2019). The Significance of Chelation Therapy in Heavy Metal Intoxication. *Journal of Heavy Metal Toxicity and Diseases*, 4, 1−10. DOI: 10.21767/2473-6457.10029

[2] ElSayed ElBastamy, E. (2018). Natural diatomite as an effective adsorbent for heavy metals in waterand wastewater treatment (a batch study). *Water Science*, 32, 32−43. DOI: 10.1016/j.wsj.2018.02.001

[3] White, P.J., Broadley, M.R. (2009). Biofortification of crops with seven mineral elements often lacking in human diets - iron, zinc, copper, calcium, magnesium, selenium and iodine. *New Phytol*, 182, 49−84. DOI: 10.1111/j.1469-8137.2008.02738 .x

[4] Elom, N.I., Entwistle, J., Dean, J.R. (2014). Human health risk from Pb in urban street dust in northern UK cities. *Environmental Chemistry Letters*, 12, 209−218. DOI: 10.1007/s1031 1-013-0436-0

[5] Salazar-Flores, J., Torres-Jasso, J.H., Rojas-Bravo, D., Reyna-Villela Z.M., Torres-Sánchez, E.D. (2019). Effects of Mercury, Lead, Arsenic and Zinc to Human Renal Oxidative Stress and Functions: A Review. *Journal of Heavy Metal Toxicity and Diseases*, 4, 1−16. DOI: 10.21767/2473-6457.10027

[6] Gu, S., Kang, X., Wang, L., Lichtfouse, E., Wang, C. (2019). Clay mineral adsorbents for heavy metal removal from wastewater: a review. *Environmental Chemistry Letters*, 17, 629−654. DOI: 10.1007/s10311-018-0813-9

[7] Elaziouti, A., Laouedj, N., Vannier, R.N. (2015). Adsorption of Congo red azo dye on nanosized SnO_2 derived from sol-gel method. *International Journal of Industrial Chemistry*, 7, 53−70. DOI:10.1007/s40090-015-0061-9

[8] Tarmizi, T., Mikha, M.C., Muhammad, S., Nurlisa, H., Ferlinahayati, F., Aldes, L. (2019). Removal of Iron(II) Using Intercalated Ca/Al Layered Double Hydroxides with $[\alpha\text{-}SiW_{12}O_{40}]_4^-$. *Bulletin of Chemical Reaction Engineering and Catalysis*, 14, 260−267. DOI: 10.9767/bcrec.14.2.2880.260-267

[9] Srinivasan, R. (2011). Advances in Application of Natural Clay and Its Composites in Removal of Biological, Organic, and Inorganic Contaminants from DrinkingWater. *Advances in Materials Science and Engineering*, 2011, 872531. DOI: 10.1155/2011/872531

[10] Gu, S., Kang, X., Wang, L., Lichtfouse, E., Wang, C. (2019). Clay mineral adsorbents for heavy metal removal from wastewater: a review. *Environmental Chemistry Letters*, 17, 629–654. DOI: 10.1007/s10311-018-0813-9

[11] Karimi, L., Salem, A. (2011). The role of bentonite particle size distribution on kinetic of cation exchange capacity. *Journal of Industrial and Engineering Chemistry*,17(1), 90−95. DOI: 10.1016/j.jiec.2010.12.002

[12] Bhattacharyya, K.G., Gupta, S.S. (2008). Adsorption of a few heavy metals on natural and modified kaolinite and montmorillonite: a review. *Advances in Colloid and Interface Science*, 140(2), 114−131. DOI: 10.1016/j.cis.2007.12.008

[13] Wang, X.H., Yang, L., Zhang, J.P., Wang, C.Y., Li, Q.Y. (2014) Preparation and characterization of chitosan-poly(vinyl alcohol)/bentonite nanocomposites for adsorption of Hg(II) ions. *Chemical Engineering Journal*, 251, 404−412. DOI: 10.1016/j.cej.2014.04.089

[14] Rao, M., Ramesh, A., Rao, G., Seshaiah, K. (2005). Removal of copper and cadmium from the aqueous solutions by activated carbon derived from Ceibapentandra hulls, *Journal of Hazardous Materials*, 129, 123−129. DOI: 10.1016/j.jhazmat. 2005.08.018

[15] Baker, H., Massadeh, A., Younes, H. (2008). Natural Jordanian zeolite: removal of heavy metal ions from water samples using column and batch methods. *Environmental Monitoring and Assessment*, 157, 319−330. DOI: 10.1007/s10661-008-0537-6

[16] Mishra, P.C., Patel, R.K. (2009). Removal of lead and zinc ions from water by low cost adsorbents. *Journal of Hazardous Materials*, 168, 319−325. DOI: 10.1016/j.jhazmat.2009.02.026

[17] Aytas, S., Yurtlu, M., Donat, R. (2009). Adsorption characteristic of U(VI) ion onto thermally activated bentonite. *Journal of Hazardous Materials*, 172, 667−674. DOI: 10.1016/j.jhazmat.2009.07.049

[18] Oliveira, L.C.A., Rios, R.V.R.A., Fabris, J.D., Sapag, K., Garg, V.K., Lago, R.M. (2003). Clay-iron oxide magnetic composites for the adsorption of contaminants in water. *Applied Clay Science*, 22, 169−177. DOI: 10.1016/S0169-1317(02)00156-4

[19] Lagergren, S. (1898). Zur theorie der sogenannten adsorption geloster stoffe, Kungliga Svenska Vetenskapsakademiens. Handlingar. *Advances in Chemical Engineering and Science*, 24, 1−39. DOI: 10.4236/jamp.2019.71001

[20] Ho, Y.S., McKay, G. (1999) Pseudo-second order model for sorption processes. *Process Biochemistry*, 34, 451−465. DOI: 10.1016/S0032-9592(98)00112-5

[21] Langmuir, I. (1916). The constitution and fundamental properties of solids and liquids. *Journal of the Chemical Society*, 38, 2221−2295. DOI: 10.1021/ja02268a002

[22] Freundlich, H., Umber, M.F. (1906). Die Adsorption in lasugen. *Journal of Physical Chemistry*, 57, 385−470. DOI: 10.12691/ijebb-5-2-1

[23] Dubinin, M.M., Zaverina, E.D., Radushkevich, L.V. (1947). Sorption and structure of active carbons. I. Adsorption of organic vapors. *Journal of Physical Chemistry*, 21, 1351−1362 . DOI: 10.4236/oalib.1103363

[24] Sdiri, A., Higashi, T., Hattab, T., Jamoussic, F., Tasea, N. (2011). Evaluating the adsorptive capacity of montmorillonitic and calcareous clays on the removal of several heavy metals in aqueous systems. *Chemical Engineering Journal*, 172, 37−46. DOI: 10.1016/j.cej.2011.05.015

[25] Eloussaief, M., Jarraya, I., Benzina, M. (2009). Adsorption of copper ions on two clays from Tunisia: pH and temperature effects. *Applied Clay Science*, 46, 409−413. DOI: 10.1016/j.clay.2009.10.008

[26] Watanabe, T. (1981). Identification of Illite/Montmorillonite Interstratifications bay X-ray Powder Diffraction. *Journal of Mineral Society of Japan*, Special Issue, 97−114. DOI:10.2465/gkk1952.15.Special_32

[27] Felhi, M., Tlili, A., Gaied, M.E., Montacer, M. (2008). Mineralogical study of kaolinitic clays from Sidi El Bader in the far north of Tunisia. *Applied Clay Science*, 39, 208−217. DOI: 10.1016/j.clay.2007.06.004

[28] Al-Asheh, S., Banat, F., Al-Rousan, D. (2002). Adsorption of copper. zinc and nickel ions from single and binary metal ion mixtures on to chicken feathers. *Adsorption Science and Technology*, 20, 849−864. DOI: 10.26717/BJSTR.2017.01.000558

[29] Samake, D. (2008). Traitement des eaux usées de tannerie à l'aide de matériaux à base d'argile. *Ph.D. Thesis*. University of Joseph Fourier, Grenoble. France. p. 167

[30] Saltalı, K., Sarı, A., Aydın, M. (2007). Removal of ammonium ion from aqueous solution by natural Turkish (Yıldızeli) zeolite for environmental quality. *Journal of Hazardous Materials*, 141, 258−263. DOI: 10.1016/j.jhazmat.2006.06.124

[31] Pelletier, M., Michot, L.J., Barrès, O., Humbert, B. (1999). Influence of KBr conditioning on the infrared hydroxyl-stretching region of saponites. *Journal of Clay Minerals*, 34, 439−445. DOI: 10.1180/000985599546343

[32] Gionis, V., Kacandes, G.D., Kastritis, I.D., Chryssikos, G.D. (2006). On the structure of the palygorskite by mid- and near-infrared spectroscopy. *American Mineralogist*, 91, 1125−1133. DOI: 10.2138/am.2006.2023

[33] Gionis, V., Kacandes, G.D., Kastritis, I.D., Chryssikos, G.D. (2007). Combined near-infrared and X-ray diffraction investigation of the octahedral sheet composition of palygorskite. *Clays and Clay Minerals*, 55, 543-553. DOI: 10.1346/CCMN.2007.0550601

[34] Madejová, J. (2003). FT-IR techniques in clay mineral studies. *Vibrational Spectroscopy*, 31, 1−10. DOI: 10.1016/S0924-2031(02)00065-6

[35] Petit, S., Robert, J.L., Decarreau, A., Besson, G., Grauby, O., Marton, F. (1995). Rapport des methods spectroscopiques à la caractérisation des phyllosilicates 2:1 Contribution of spectroscopic methods to 2:1 clay characterization. *Bulletin des centres de recherches exploration-production Elf-Aquitaine*, 19, 119−147. DOI: 10.3406/argil.1969.1105.

[36] Sysa, L.V., Stepova, K.V., Petrova, M.A., Kontsur A.Z. (2019). Microwave-treated bentonite for removal of lead from wastewater, *Voprosy khimii i khimicheskoi tekhnologii*, 5, 126-134. DOI: 10.32434/0321-4095-2019-126-5-126-134.

[37] Dafalla, M., Al-Mahbashi, A., Al-Shamrani, M. (2018). Trends of Moisture and Electrical Conductivity in Clay Liners. *Geofluids*, 2018, 8391830. DOI: 10.1155/2018/8391830.

[38] Ho, Y.S., McKay, G. (1999). Pseudo-second order model for sorption processes. *Process Biochem*, 34, 451−465. DOI: 10.1016/S0032-9592(98)00112 -5

[39] Koffi, L.K., Claire, P., Jean-Pierre, B., Agnès, S., Alain, J., Patrick, M., Philippe, A. (2007). Surface properties of kaolin and illite suspensions in concentrated calcium hydroxide medium. *Journal of Colloid and Interface Science*, 307, 101−108. DOI: 10.1016/j.jcis.2006.10.085

[40] Arib, A., Sarhiri, A., Moussa, R., Remmal, T., Gomina, M.C.R. (2007). Caractéristiques structurales et mécaniques de céramiques à base d'argile. *Comptes Rendus Chimie*, 10, 502-510. DOI: 10.1016/j.crci.2006.12.009

[41] Rouff, A.A., Elzinga, E.J., Reeder, R.J., Fisher, N.S. (2006). The effect of aging and pH on Pb(II) sorption processes at the calcite–water interface. *Environmental Science and Technology*, 40, 1792−1798. DOI: 10.1021/es051523f

[42] Giles, C.H., Mac Ewan, T.H., Nakhwa, S.N., Smith, D. (1960). Studies in adsorption. Part XI. A. system of classification of solution adsorption isotherms, and its use in diagnosis of adsorption mechanisms and in measurement of specific surface areas of Solids. *Journal of the Chemical Society*, 1960, 3973−399. DOI: 10.1039/JR9600003973

[43] Sari, A., Tuzen, M., Citak, D., Soylak, M. (2007). Equilibrium.kinetic and thermodynamic studies of adsorption of Pb(II) from aqueous solution onto Turkish kaolinite clay. *Journal of Hazardous Materials*, 149, 283−291. DOI: 10.1016/j.jhazmat.2007.03.078

[44] Onyango, M.S., Kojima, Y., Aoyi, O., Bernardo, E.C., Matsuda, H. (2004). Adsorption equilibrium modeling and solution chemistry dependence of fluoride removal from water by trivalent-cation-exchanged zeolite F-9. *Journal of Colloid and Interface Science*, 279, 341−350. DOI: 10.1016/j.jcis.2004.06.038

[45] Khalifa, A.Z., Özlem, C., Pontikes,Y., Heath, A., Patureau, P., Bernal, S.A., Marshc, A.T.M. (2020). Advances in alkali-activation of clay minerals. *Cement and Concrete Research*, 132, 106050. DOI: 10.1016/j.cemconres.2020.106050

[46] Sarkar, B., Xi, Y., Megharaj, M., Krishnamurti, G.S.R., Naidu, R. (2010). Synthesis and characterisation of novel organopalygorskites for removal of p-nitrophenol from aqueous solution: isothermal studies. *Journal of Colloid and Interface Science*, 350 295−304. DOI: 10.1016/j.jcis.2010.06.030

[47] Bhattacharyya, K.G., Gupta, S.S. (2006). Pb(II) uptake by kaolinite and montmorillonite in aqueous medium: influence of acid activation of the clay. *Colloids and Surfaces A*, 277, 191−200. DOI: 10.1021/ie061475n

[48] Chaari, I., Fakhfakh, E., Chakroun, S., Bouzid, J., Boujelben, N., Feki, M., Rocha, F., Jamoussi, F. (2008). Lead removal from aqueous solutions by a Tunisian smectitic clay. *Journal of Hazardous Materials*, 156, 545−551. DOI: 10.11648/j.css.20170204.12

[49] Eloussaief, M., Benzina, M. (2010). Efficiency of natural and acid-activated clays in the removal of Pb(II) from aqueous solutions. *Journal of Hazardous Materials*, 178, 753−757. DOI: 10.1016/j.jhazmat.2010.02.004

[50] Kaya, A., Hakan Ören, A. (2005). Adsorption of zinc from aqueous solutions to bentonite. *Journal of Hazardous Materials*, 125, 183−189. DOI: 10.1016/j.jhazmat.2005.05.027

[51] Oruh, S.C. (2008). The removal of zinc ions by natural and conditioned clinoptilolites, Desalination. *Progress and Sustainable Energy*, 225, 41−57. DOI: 10.1002/ep.12260

[52] Ulmanu, M., Mara˜nón, E., Fernández, Y., Castrillón, L., Anger, I., Dumitriu, D. (2003). Removal of copper and cadmium ions from diluted aqueous solutions by low cost and waste material adsorbents. *Water Air and Soil Pollution*, 142, 357−373. DOI: 10.1002/ep.12583

[53] Murray, H.H. (2007). *Applied Clay Mineralogy: Occurrences. Processing and Application of Kaolins-Bentonites-Palygorskite-Sepiolite and Common Clays*, first edition., UK: Elsevier Science Ltd. p.189.